Determining the Volume of a Surface Defined by Tomographic Scattering Points

University of Science and Arts of Oklahoma
Dao Thong Lim, Laura Bennett, Rachel Bennett
Jordan Danser, Shauntel Cornaby

May 5, 2015

Background

The imaging of materials through the use of scattered photons is an area of active research in the medical field. A number of techniques for data collection and image reconstruction exist, such as x-ray tomography, in which a beam of low energy x-rays are passed through an object and the change in intensity of the beam as it comes out (caused by Compton scattering or absorption as the beam interacts with materials within the target) is measured. The physical setup and geometry of the x-ray and detectors varies, with many systems sending out either a pencil-shaped singular beam or a fan-shaped beam. For most modern systems, a single x-ray source fixed on a rotating ring is passed around a target's central axis, capturing a number of images over 360° as the detector moves along the length of the target [**?**]. Cone beam scanning, a method used primarily in dentistry, utilizes a conical array of x-ray beams to capture a full 360° in only one pass [**?**]. Another heavily researched method is microwave imaging via space-time beamforming (MIST) [**?**], in which a transmitting antenna sends electromagnetic radiation in the microwave spectrum into a target and a scanning antenna records the scattering of individual photons off of anomalies within the target (e.g. a tumor within breast tissue). This can be done with an array of antennas arranged in a circle about the target, with each antenna sequentially acting as an emitter while the others act as receivers [**?**]. The data may be processed via computerized tomography, which divides the target into individual slices (*tomos*) with a certain thickness, then processes the individual volume elements (voxels) of each slice; each voxel is assigned an attenuation coefficient, which is a measure of the proportion of the beam that is scattered or absorbed by the material enclosed within the voxel. A higher degree of attenuation (higher attenuation coefficient) reflects either a denser material or a material with a high atomic number; tumors are more likely to have higher attenuation than surrounding tissues given their abnormal density, causing a larger amount of photon scattering.

Problem Statement

The problem addressed in this project is: given a set of scattering points with coordinates (x, y, z), can the volume of the tumor that gave rise to the elements be determined?

The data is given by a random sampling of scattering points located within the region of interest. The beam that produces the scattering decays as it passes through a material; its strength is given by the function

$$S(x) = Ae^{-\alpha x} \tag{1}$$

Where A is the cross-sectional area of the beam, α is the attenuation coefficient, and x is the depth of the target object (or, alternatively, the path length of the beam through the object). This implies that the scattering is more likely to occur close to the surface of a dense object (such as a tumor) than deep within it. The attenuation coefficient, a measure of how much the intensity of the beam used will be reduced as it passes through some material, will vary depending on the density and chemical makeup of the region. A higher attenuation coefficient implies that the material will cause a rapid loss in intensity of the beam; bones and tumors are examples of materials that have higher attenuation coefficients. For this project, α was expected to range between 0.6 and 1.4.

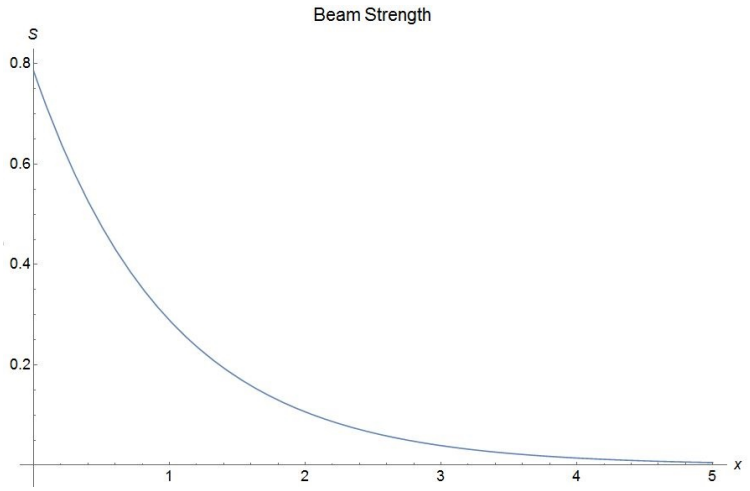

Figure 1: The strength of the beam (y axis) decays with increasing depth (x axis). Here, the image is given by a beam with area 0.8 mm and α of 1.

Procedure and Methodology

The primary tool used in addressing this problem was Mathematica version 10, with which we were able to do complex computational analysis and data generation, and convex set theory.

In order to derive volumes from our scattering points, we used the concept of convex hulls and Mathematica's ConvexHullMesh function. A convex hull of a set of points is defined as the smallest convex set in euclidean space that contains those points. The algorithm used by Mathematica to compute the convex hull was a variation of the Quickhull algorithm [**?**].

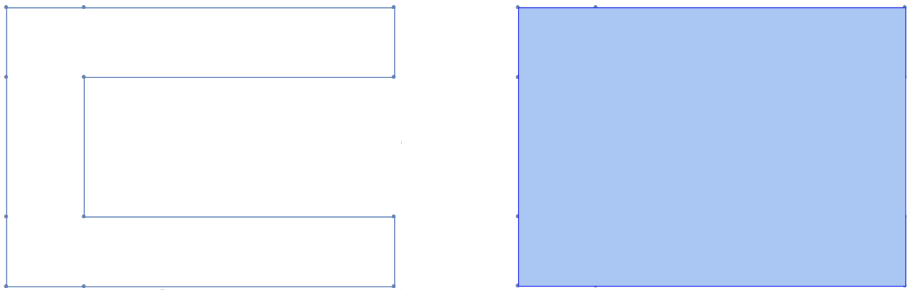

Figure 2: On the left is a set of points; on the right, the convex hull of that set.

To simplify the problem, we made the following assumptions: (1) because benign tumors are typically regular in shape, we used a sphere as our primary model for a tumor; (2) all radiation beams are directed toward the center of mass of the tumor. We also considered slightly less regular shapes such as the ellipsoid and the cylinder. With those shapes, radiation beams were directed toward a central axis as opposed to the center of mass of the shape. This is similar to how most modern systems work.

There are, however, limitations and further considerations that need to be tested and analyzed beyond the scope of our work. For instance, malignant tumors tend to be irregular in shape thus possibly containing cusps and voids. Our algorithm does not deal with these conditions optimally. Also, our models of tumors are all strategically placed (such as being centered at the origin where radiation beams are directed, or placed in such a way that photon beams are directed toward a central axis that runs down the middle of the length of the model) to give optimum scattering points. Generalizing the placement of the tumors was not thoroughly analyzed and is left for further research.

Additionally, it was necessary to generate our own data for the problem using objects with known dimensions in order to simulate the sampling beam and check the accuracy of our algorithms. A description of our methodology follows.

Generation of Sample Data

The first step was to generate objects with known dimensions to test our algorithm. The shapes that were primarily used were a sphere, an ellipsoid, and a cylinder. We assumed our data to be representative of benign tumors, which are generally more spherical and regular than malignant tumors [**?**]; as such, we did not encounter cusps and voids, a problem which requires additional research.

For a sphere with radius r, our control data was generated by finding random values between -1 and 1 for x_0, y_0, and z_0. We determined the unit vector defined by these points and scaled it according to the radius r of the sphere, exclusively generating points on the surface defined by the vector

$$\vec{p}(x_0, y_0, z_0) = \frac{r}{\sqrt{x_0^2 + y_0^2 + z_0^2}} \langle x_0, y_0, z_0 \rangle$$

.

The ellipsoid, defined by the equation

$$\frac{x^2}{a^2} + \frac{y^2}{b^2} + \frac{z^2}{c^2} = 1$$

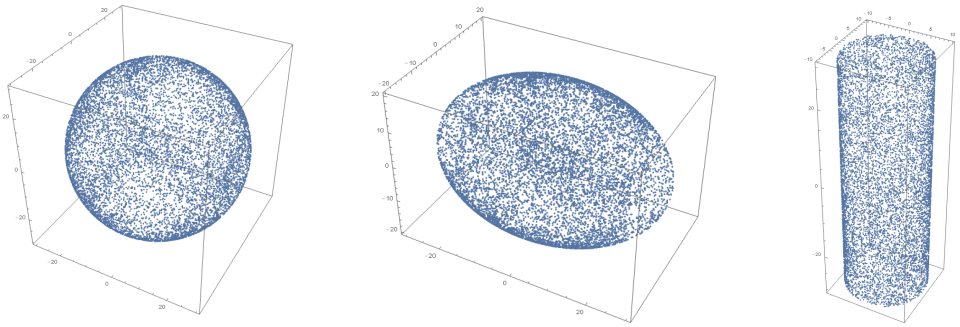

Figure 3: Generated surface points for the sphere, cylinder, and ellipse

where a, b, and c are constant, was generated by first generating random values x_0 and z_0 between -1 and 1 and y_0 between $-b$ and b. In order to scale the values to the surface of the ellipsoid, we calculated a value t such that

$$\frac{x_0^2 t^2}{a^2} + \frac{y_0^2}{b^2} + \frac{z_0^2 t^2}{c^2} = 1$$

Where solving for t yields

$$t = \sqrt{\frac{1 - (\frac{y_0}{b})^2}{(\frac{x_0}{a})^2 + (\frac{z_0}{c})^2}}$$

and multiplying x_0 and z_0 by this value will produce a vector $\langle x_0 t, y_0, z_0 t \rangle$ that designates a random point on the surface of the ellipsoid. This model will use the y-axis as the axis the photon beams are directed toward.

For the bases of a cylinder running along the z-axis, random x and y values between $-r$ and r were generated and retained only when they were found to lie within the circle defined by

$$x^2 + y^2 \leq r^2$$

where r is the radius of the cylinder and x and y are randomly generated numbers. A value $z = \frac{1}{2}h$ (where h is defined as the height of the cylinder) was created and randomly assigned to one of the bases. For the side of the cylinder, a process similar to that of the sphere was utilized: random x and y values between -1 and 1 were generated to create a vector $\langle x, y \rangle$ then rescaled to attain a vector of magnitude r defining points on the surface of the cylinder. A random height z between $-\frac{1}{2}h$ and $\frac{1}{2}h$ was then generated and assigned to the point.

For each shape, 10,000 points were generated and sampled from.

Beam Simulation

In practice, scattering does not occur exclusively on the surface of a tumor; instead it tends to scatter below the surface at a depth that is dependent on the material's chemical makeup and density. The strength of the beam (or its ability to penetrate the object) decays at a rate of $S(x) = Ae^{-\alpha x}$. To simulate the effects the interaction of the tumor and the photon

beam have on the amount and location of scattering at some depth near the surface, we randomly generate a two dimensional point $(x, y) \in [0, \infty) \times [0, \infty)$.

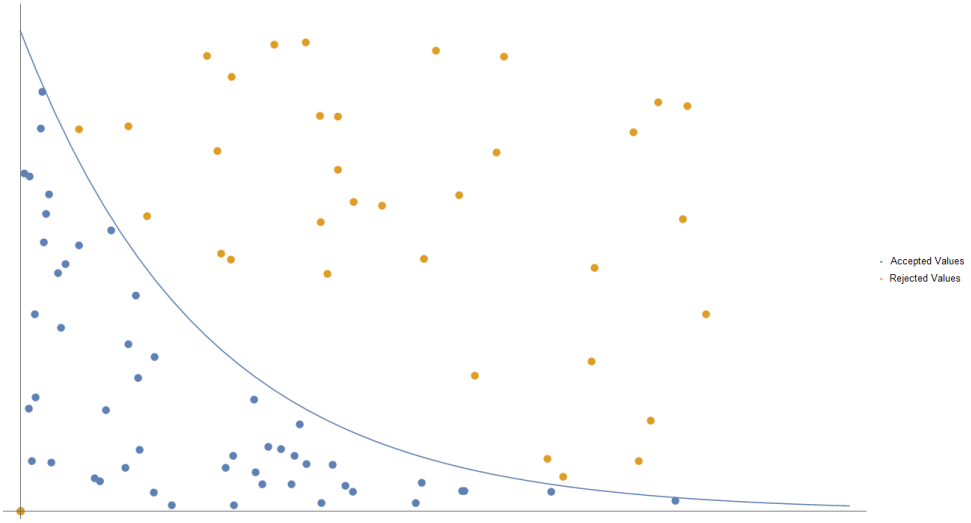

Figure 4: Generation of points for beam simulation. Blue points are those that are accepted, while orange points are rejected.

If point (x, y) lies below the decay curve S, we define a scattering point p to be the point a distance x from a given control surface point q in the direction of the center of mass (or center axis) of the dense object. If (x, y) lies above the decay curve S, we randomly generate another (x, y) point until one is below the curve S. We do this for each random point on the control surface. Since a point (x, y) has a higher chance of lying below S when x is near 0 than when it is near r, nearly all of the scattering points will be slightly below the surface of the tumor or dense object.

Approximation of the Sphere

A tumor that develops by diffusion alone can be assumed to grow spherically [**?**]. Under this assumption, we examined a number of properties for our spherical model, finding an approximation for the actual volume using these properties.

For a given attenuation coefficient, α, the mean penetration depth for a photon entering the sphere was found to be

$$\mu = \int_0^\infty \frac{xe^{-\alpha x}}{\int_0^\infty e^{-\alpha x} dx} dx$$

with a standard deviation of

$$\sigma = \sqrt{\int_0^\infty (x - \mu)^2 \frac{e^{-\alpha x}}{\int_0^\infty e^{-\alpha x} dx} dx}$$

Because the scattering points would occur some distance below the surface of the sphere, the convex hull of the simulated beam data would produce an underestimate. Because the penetration depth of the scattering points depends only on the attenuation constant α, the volume $V_c(\alpha)$ of the convex hull produced by the scattering points is also dependent only on

α. Therefore, the percentage $P(\alpha, r)$ of the volume captured by the convex hull of the beam data compared to the volume of the control (a sphere of radius r) is given by

$$P(\alpha, r) = \frac{V_c(\alpha)}{V_0(r)} \tag{2}$$

$P(\alpha, r)$ was found to be linearly correlated to the attenuation α and the radius of the control sphere r with a correlation coefficient of $R = .965$.

Comparing the results of a series of trials for varying r and α shows the linear trend for $P(\alpha, r)$ can be empirically approximated by

$$P'(\alpha, r_{est}) = 0.213 r_{est} + 1.486\alpha + 93.491$$

In this case, r_{est} is the estimated value for r, given by

$$r_{est} = r_{avg} + \mu$$

where r_{avg} is the average of the distance between all points generated in the beam simulation and the center of mass generated by those points. Because the scattering tends to occur below the surface of the target, the average penetration depth μ must be added to approximate the actual radius r.

Using r_{est}, $P'(\alpha, r_{est})$, and equation (**??**), we can derive an approximation $V_{est}(\alpha, r_{est})$ for the actual volume $V_0(r)$,

$$V_{est}(\alpha, r_{est}) = \frac{V_c(\alpha)}{P'(\alpha, r_{est})}$$

α \ r	2	6	10	14
0.6	94.34%	95.95%	96.83%	97.31%
0.8	94.55%	95.92%	97.29%	97.68%
1	95.37%	96.49%	97.50%	97.94%
1.2	95.52%	96.88%	97.73%	98.11%
1.4	95.66%	96.97%	97.94%	98.27%

(a) Values for $\frac{V_c(\alpha)}{V_0(r)}$

α \ r	2	6	10	14
0.6	99.46%	101.43%	100.17%	99.01%
0.8	99.83%	101.31%	100.07%	99.17%
1	100.35%	101.33%	100.16%	99.87%
1.2	100.82%	101.18%	100.32%	100.51%
1.4	101.09%	101.07%	100.50%	101.31%

(b) Values for $\frac{V_{est}(\alpha, r_{est})}{V_0(r)}$

Figure 5: Average percentages of volumes captured over fifteen trials for a given r and α

Figure **??** shows that dividing the volume of the convex hull $V_c(\alpha)$ by the associated percentage given by $P'(\alpha, r_{est})$ results in a more accurate approximation of the volume. For tumors whose shapes are nonspherical, such as an ellipsoid or a cylinder, the volume V_0 is dependent on multiple parameters and thus more difficult to get a handle on. As a result, the percentage of the volume of the convex hull of the scattering points to the actual volume is dependent on multiple parameters depending on its shape. Therefore, an approach similar to the one used for the sphere is difficult and requires further research. $V_c(\alpha)$ remains our best approximation, noting that it is an under approximation.

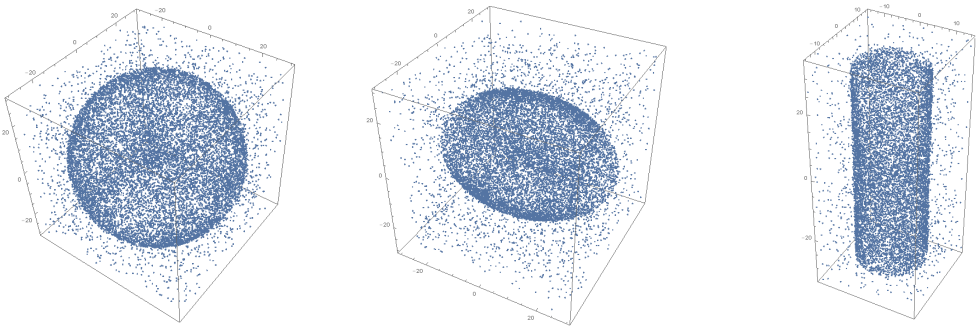

Figure 6: Square, ellipsoid, and cylinder with noise.

Noise

In reality, the data obtained from a tomographic scan will contain a significant amount of noise. Noise is defined as irregularities in data that could obscure the signal; for our purposes, it is any registered scattering element that does not originate in the tumor. This can occur when a tumor is located within or near tissues with different attenuation constants, causing some degree of scattering, making it difficult to distinguish between tissues of interest and the surrounding tissues (e.g. differentiating between bone and tumors). In order to best simulate the scattering process, it was necessary to generate a certain amount of random noise. Signal-to-noise ratio typically ranges from 1:1 to 4:1.

Currently, our algorithm is unable to distinguish between different objects optimally; further work would need to be done to find a more sophisticated solution.

Noise Elimination

After generating the simulated beam data and adding noise, it was then necessary to filter the data and determine the volume enclosed by the points. In order to filter out some of the noise while retaining the more valuable data, we first divided the region into a three dimensional grid of equally-sized voxels (3-dimensional pixels). We then determined the number of points that were found in each voxel, storing the value in an array. Because tumors tend to be more dense than the surrounding tissue or region, a threshold value was determined and used to find voxels containing scattering points of the tumor - for example, a voxel containing more than six data points was considered a *tumor voxel*. The average point of all the points in each tumor voxel was determined and plotted. These new points served as representative points for the tumor; convex hulls were created from them, and the location of the center of mass and volume of the newly generated surfaces were calculated using built-in functions in Mathematica.

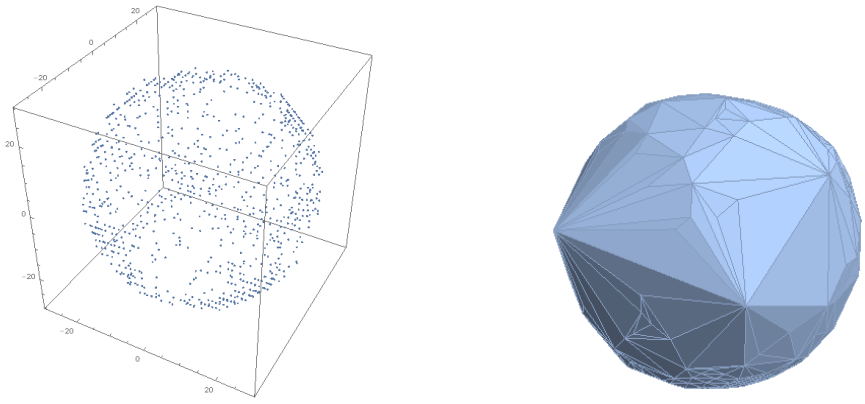

Figure 7: Voxel points of the sphere and accompanying convex hull

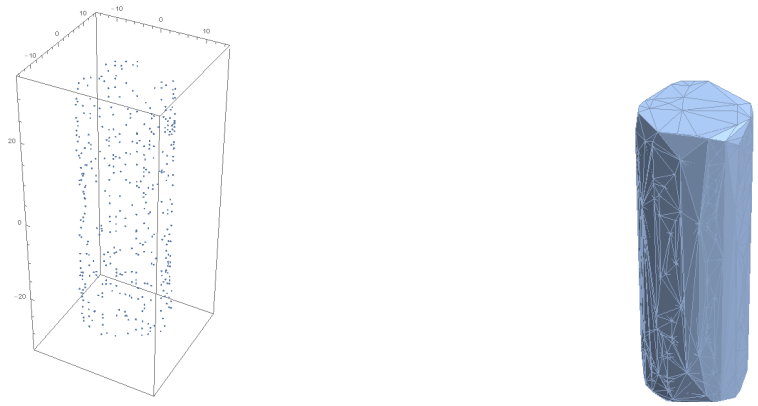

Figure 8: Voxel points of the cylinder and accompanying convex hull

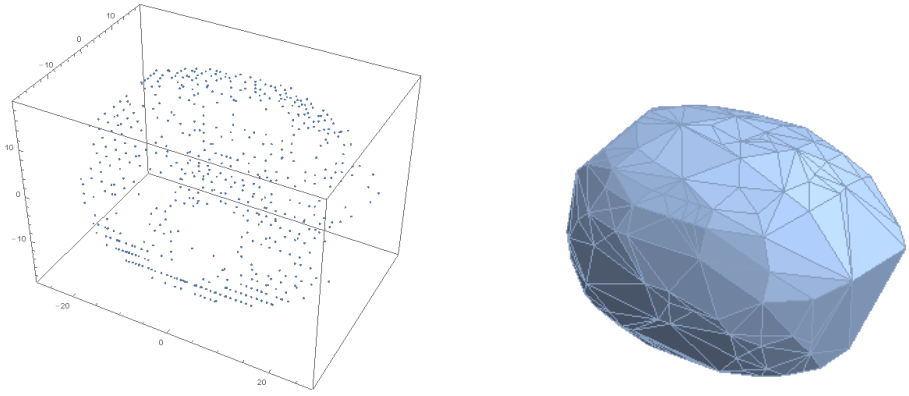

Figure 9: Voxel points of the ellipsoid and accompanying convex hull

Results

For the sphere with voxels, which could be adjusted with the procedure described in the Approximation of the Sphere section, the resulting percentages were closer to the actual volume than $V_c(\alpha)$; however, the correlation coefficient for $P(\alpha, r)$ was $R = .762$, and our values for $P'(\alpha, r_{est})$ were therefore not as accurate as they were without noise. The empirical equation for the estimated percentage of volume captured was

$$P'(\alpha, r_{est}) = 1.124r_{est} + 6.055\alpha + 69.576$$

Despite the lower correlation between r, α, and P, the volume captured after factoring in $P'(\alpha, r_{est})$ showed marked improvement when compared to the values for $P(\alpha, r)$.

α \ r	2	6	10	14
0.6	71.32%	85.75%	86.98%	82.67%
0.8	73.33%	87.55%	88.95%	86.14%
1	72.16%	88.02%	89.72%	88.34%
1.2	74.90%	89.34%	91.09%	90.00%
1.4	73.81%	90.05%	91.60%	90.81%

(a) Values for $\frac{V_c(\alpha)}{V_0(r)}$

α \ r	2	6	10	14
0.6	92.69%	106.84%	102.13%	92.05%
0.8	94.37%	107.59%	103.14%	94.86%
1	91.75%	106.63%	102.73%	96.12%
1.2	94.00%	106.62%	102.97%	96.74%
1.4	91.39%	105.93%	102.16%	96.43%

(b) Values for $\frac{V_{est}(\alpha, r_{est})}{V_0(r)}$

Figure 10: Average percentages of volumes captured over fifteen trials for a given r and α.

When comparing the captured voxel volumes $V_c(\alpha)$ with the control convex hulls, the results were consistently above 85%.

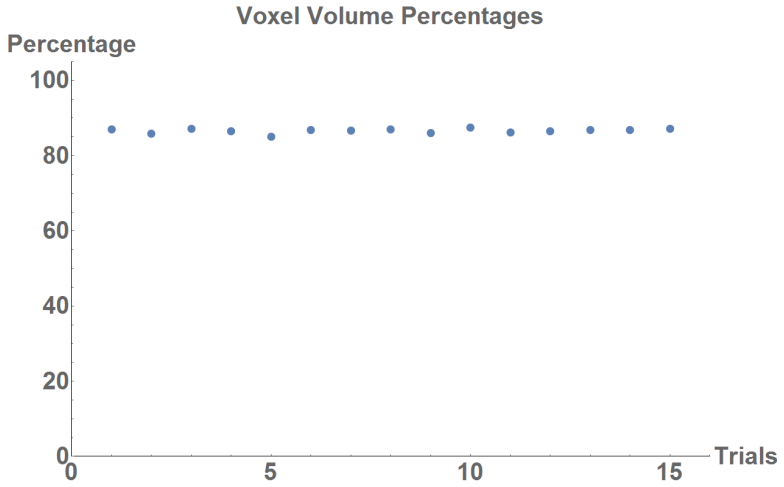

Figure 11: Average volume captured with the cylinder's convex hull

For the cylinder, the average volume was 87% for an α of 0.6.

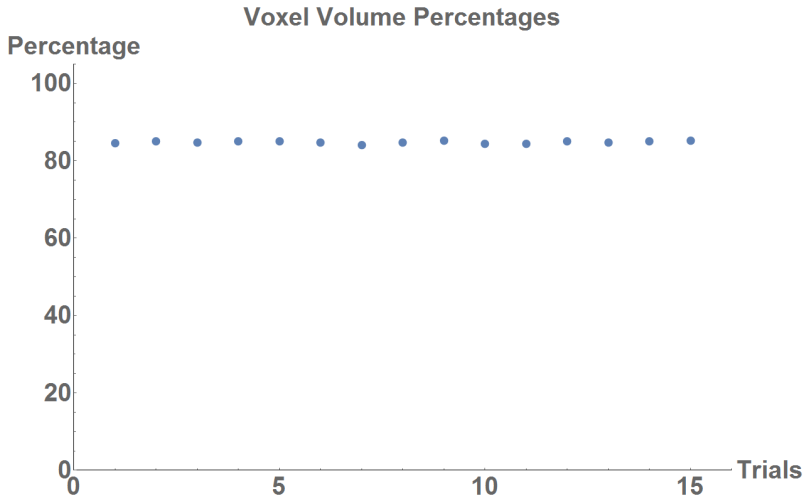

Figure 12: Average volume captured with the ellipsoid's convex hull

For the ellipsoid, the average volume contained was 85% for an α of 0.6.

As it stands, the approximation $V_c(\alpha)$ remains our best approximation for the volume of non-spherical shapes. This is because the standard deviation σ is equal to the average penetration depth μ, and as such a number of points would lie close to the surface of the object a distance σ beyond μ toward the surface; since the convex hull is only based on the outermost points of a set, this was sufficient to produce a decent approximation of the original shape.

Conclusion

Given a set of scattering points, we were able to reconstruct at least 85% of the volume of a given target. Additionally, we were able to filter a significant amount of random noise from the data while still retaining much of the original volume. For spherically shaped targets, we were able to estimate the radius of the target and, through statistical analysis, determined an empirical relationship between α, r, and the percentage ($P'(\alpha, r)$) of volume captured that allowed us to estimate up to 100% of the actual volume.

Areas that will require further research include adapting our algorithm for more irregularly shaped objects in order to better simulate malignant tumors; differentiating between materials with different attenuation coefficients; and revising our data acquisition such that it better models the way modern imaging devices collect data.

References

[1] Richard A Ketcham and William D Carlson. Acquisition, optimization and interpretation of x-ray computed tomographic imagery: applications to the geosciences. *Computers & Geosciences*, 27(4):381–400, 2001.

[2] William C Scarfe, Allan G Farman, and Sukovic Predag. Clinical applications of cone-beam computed tomography in dental practice. *Journal of the Canadian Dental Association*, 72(1):75–80, 2006.

[3] Essex J Bond, Xu Li, Susan C Hagness, and Barry D Van Veen. Microwave imaging via space-time beamforming for early detection of breast cancer. *Antennas and Propagation, IEEE Transactions on*, 51(8):1690–1705, 2003.

[4] Amir H Golnabi, Paul M Meaney, Shireen D Geimer, and Keith D Paulsen. Comparison of no-prior and soft-prior regularization in biomedical microwave imaging. *Journal of medical physics/Association of Medical Physicists of India*, 36(3):159, 2011.

[5] C. Bradford Barber, David P. Dobkin, and Hannu Huhdanpaa. The quickhull algorithm for convex hulls. *ACM Trans. Math. Softw.*, 22(4):469–483, December 1996.

[6] Robin N Strickland, editor. *Image-Processing Techniques for Tumor Detection*. Mercel Dekker Inc, New York, NY, 2002.

[7] HP Greenspan. Models for the growth of a solid tumor by diffusion. *Stud. Appl. Math*, 51(4):317–340, 1972.